

2022 NA62 Status Report to the CERN SPSC

Abstract

The status of the NA62 experiment is reported. The current status of detectors and hardware is summarised, together with our experience of the 2021 data taking. Plans for the 2022 data taking and Run2 (2022–2025) are presented. Highlights of rare and forbidden decay analyses and exotic searches are also discussed.



1 Introduction

The NA62 experiment has been approved by the CERN Research Board to continue the data taking during the period after CERN Accelerators Long Shutdown 2 (LS2) and until Long Shutdown 3 (LS3). The experiment is strongly committed to reaching its physics goals for the upcoming years, which are: to complete the measurement of the branching ratio of the ultra-rare $K^+ \rightarrow \pi^+ \nu \nu$ decay as proposed; to substantially increase the sensitivity to several rare and forbidden kaon decays; and reach unprecedented sensitivity in the investigation of several Standard Model (SM) extensions involving feebly interacting long-lived particles. The Finance Review Committee of November 2021 approved the budget for 2022, and the forecast for 2023.

Since the previous report in April 2021 [1], the NA62 experiment has completed the beam line modifications, the preparation and installation of new detectors, and has successfully taken data in the Summer and Autumn of 2021 reaching nominal beam intensity, fulfilling important targets for the 2021 data-taking. Several results on rare and exotic processes have been achieved, and published. This report offers a status report on the experiment and data collected in 2021, and presents our plans for NA62-Run2. Several physics analyses are ongoing, spanning precision measurements and searches for exotic processes.

The document is structured as follows: Sections 2, 3, 4 and 5 summarise the activities on the beam, hardware, the data quality and simulation; the status of the $K^+ \rightarrow \pi^+ \nu \bar{\nu}$ analysis using the 2021 data, and plans for Run2 are described in Section 6. Sections 7 and 8 report current highlights of rare/forbidden decays and exotic searches, respectively. Finally, the list of recent publications is presented in Section 9.

2 Beam and spill structure

The 2021 data taking suffered from a period of about two weeks with no hadron beam to NA62, and then several problems with the beam tuning in K12, that was also affected by instrumentation issues. Intensity on T10 reached about 50-60% of nominal in August, and remained so due to low T4-to-T10 transmission. From early September, the number of particles delivered by the SPS per burst, as measured by the T10 and Argonion counters, was increased to, and maintained at, approximately 100% of the nominal NA62 specification. The T10 value for nominal intensity was newly defined in 2021 as about 40-45 units, rather than the expected 33 units, based on the observation of Argonion counts and NA62 detectors. This highlights the need of a trustworthy, independent instrument that can be used to record the protons on T10 target. Several problematic periods of beam absence and instability were still present throughout the year, including a series of issues with stability of beam magnets related to faulty regulation cards in power converters. The data taking concluded in mid November.

The quality of the extracted proton beam spill remained problematic for the entire data taking period. Specifically, detailed studies of the spill structure, as observed by the NA62 detectors, have demonstrated that the instantaneous intensity delivered to NA62 was significantly higher within approximately the first second of the spill, i.e. corresponding to a timestamp from the Start-Of-Burst (SOB) signal $t < 2$ s (the proton extraction only starts at $t = 1$ s). There was significant effort spent in characterising the first second in the spill. It appears that the unsustainable high rates in our detectors are caused by intervals of anomalously high beam currents. Investigations have been performed using both triggered data and trigger primitive information. In both cases, the distribution of the time of the event (or the primitive) as a function of the modulus of the time with respect to the revolution frequency of the SPS (folded event timestamp, in units of 25 ns) has been produced. Fig. 1 (left) shows the distribution of the folded phase versus time in burst from primitive data, which shows an anomalous behaviour below 2 seconds (y axis) while above 2 seconds the structure of the spill is as expected. A zoom

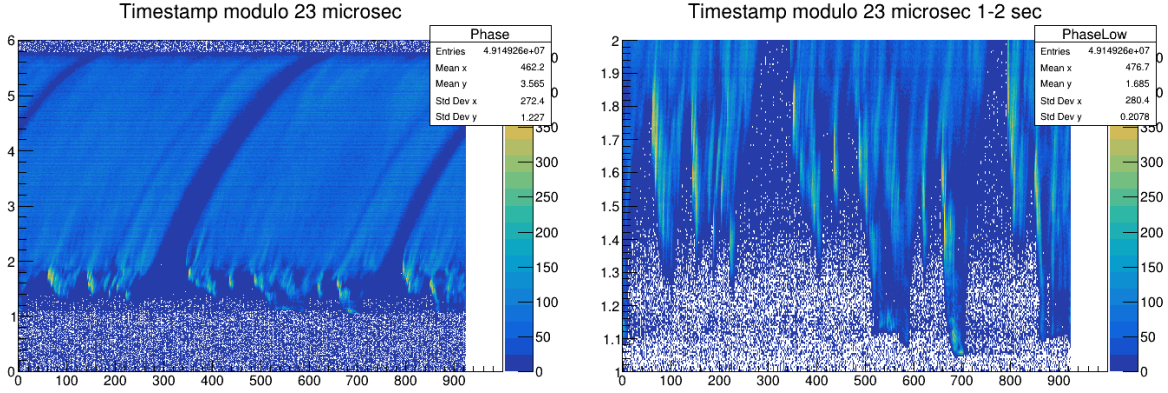


Figure 1: Distributions of events in the spill from SOB vs folded event timestamp in units of 25 ns, all events (left) and events within the first second in the spill (right).

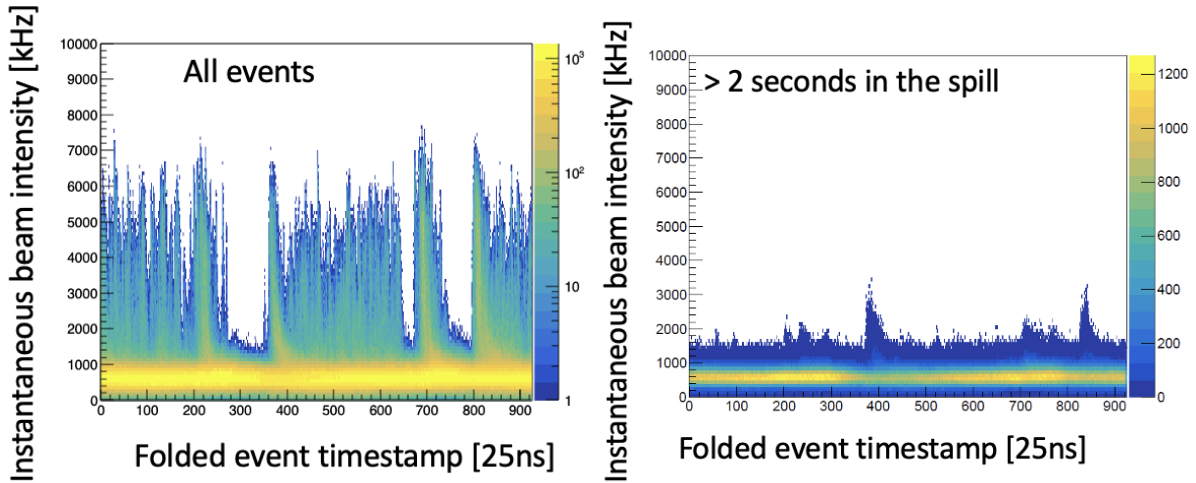


Figure 2: Distributions of instantaneous intensity vs folded event timestamp in unit of 25 ns, all events (left) and events after 2 sec in the spill (right). The color scale indicates the occupancy of each (folded event timestamp, intensity) bin.

of the region below 2 seconds is shown in Fig. 1 (right): a “filament” structure can be seen with high rate of events in specific regions. Distributions of instantaneous intensity seen with GTK hits in events where the number of hits saturates the recording buffer versus folded timestamp (Fig. 2) show clearly that before 2 seconds there are high-intensity intervals up to about 8 times the nominal one, without a strong correlation with specific values of the phase.

These high-intensity intervals produce saturation of readouts, trigger and data acquisition systems, causing a sizeable loss of data, and repercussions (like dead time, reset time etc.) beyond their duration. Ultimately the quality of the spill structure severely limited the percentage of protons which could be used for physics in 2021.

Possible origins of the effect and ways to improve the spill structure are being discussed with the CERN BE-OP and BE-EA groups. New tools from NA62 are being developed, together with beam experts, to give a fast feedback on the spill structure and quality to the operation team during the beam tuning phase in 2022. If this effect cannot be substantially reduced, other strategies are being considered, including the possibility of delaying the extraction by 1 sec and correspondingly extending the spill duration.

NA62 is grateful for the commitment of CERN in delivering a high-intensity beam to NA62 and for the efforts to improve the spill structure.

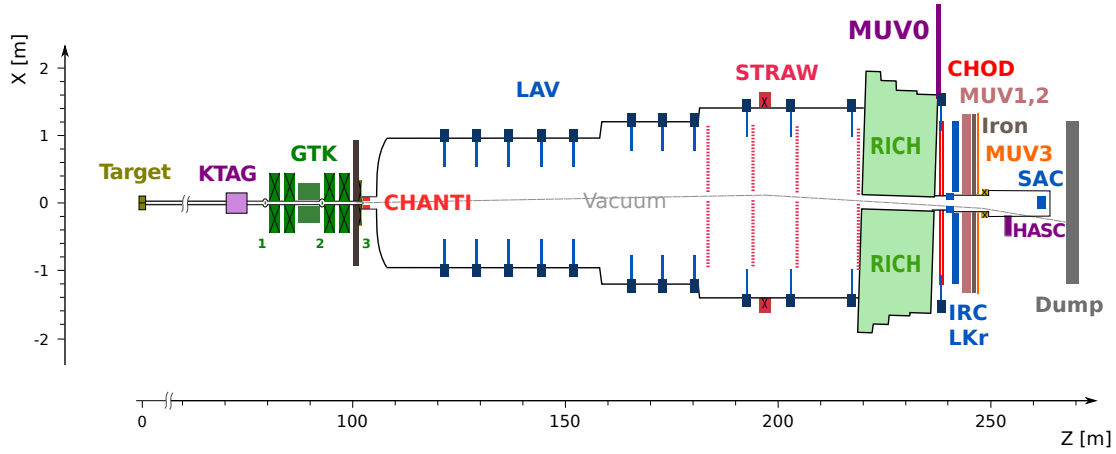


Figure 3: Layout of the NA62 experiment. KTAG: differential Cherenkov counter; GTK: Si pixel beam tracker; CHANTI: ring stations of scintillator bars; LAV: lead glass ring calorimeters; STRAW: straw magnetic spectrometer; RICH: ring imaging Cherenkov counter; MUV0: off-acceptance plane of scintillator pads; CHOD: planes of scintillator pads and slabs; IRC: inner ring shashlik calorimeter; LKr: electromagnetic calorimeter filled with liquid Krypton; MUV1,2: hadron calorimeter; MUV3: plane of scintillator pads for muon veto; HASC: near beam lead-scintillator calorimeter; SAC: small angle shashlik calorimeter. In the layout, the final fixed collimator installed in 2018 is visible, between GTK and CHANTI.

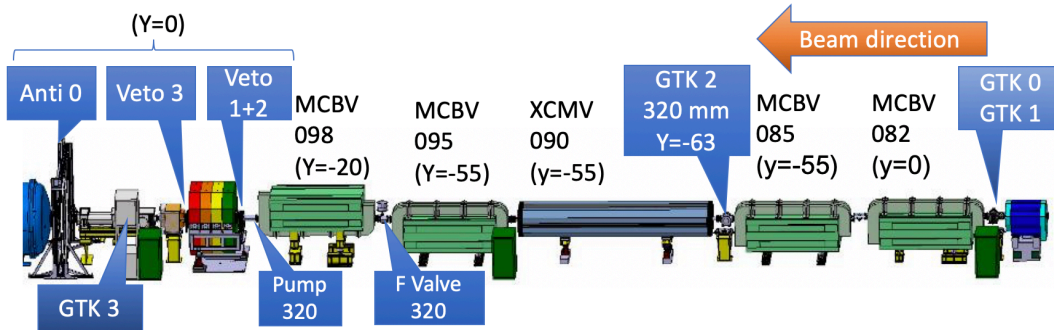


Figure 4: Schematic layout of the new achromat and beam line.

3 Status of the detector and on-going activities

A description of the detector can be found in Ref. [2], and is schematically shown in Fig 3. In order to reduce the background contamination to the measurement of the $K^+ \rightarrow \pi^+ \nu \nu$ decay, the beam layout upstream of the decay volume has been modified during LS2 [1]. The main changes are: an optimized achromat; a 4th GTK station (GTK0) placed next to GTK1; a new veto-counter (VetoCounter) around the beam pipe before and after the collimator. In addition, a new hodoscope (Anti0) has been installed mainly to reduce the muon halo background present in dump mode searches; and the HASC has been duplicated in a symmetrical position with respect to the beam axis to act as a photon veto complementary to the LAV, LKr, IRC and SAC calorimeters. The new beam layout upstream of the fiducial volume is shown in Fig. 4.

3.1 New Detectors

The VetoCounter was designed to significantly suppress upstream backgrounds from kaon decays occurring upstream of the fiducial volume, specifically between the GTK2 and final collimator. These background mechanisms form the majority of the total ‘upstream background’, which in turn has been the largest background for the $K^+ \rightarrow \pi^+ \nu \bar{\nu}$ analysis [3]. The VetoCounter is formed from three parallel planes of scintillating tile detectors: two before the final collimator, (VC1,2) separated by a 25 mm lead sheet, and one after the final collimator (VC3). The VetoCounter detector was commissioned during the 2021 data-taking, with VC1 and VC2 installed in early August and VC3 installed in mid September. Delays in production and delivery of electronic devices caused by the pandemic meant that in 2021 the VetoCounter had to make use of constant fraction discriminators (CFDs) that were available at UCLouvain but were originally designed for a different purpose. As a consequence, the CFD thresholds were at non-optimal levels to protect the electronics from high pulse amplitudes, thereby reducing the efficiency of the detector. In 2022 new CFDs will be used, together with a new motherboard: the final production of the CFDs has been completed, while there have been minor delays in the production of the motherboard. The installation of both is expected in April 2022.

The Anti0 hodoscope was designed mainly to reduce the background present in dump mode searches. The detector consists of two planes of scintillating tiles readout by silicon photo-multipliers. It was installed at the entrance of the fiducial volume and commissioned during the 2021 data-taking.

A second HAdronic Sampling Calorimeter (HASC2) station has been installed, mirroring the original HASC station, resulting in a symmetric detector at the end of the beam-line.

With continued CERN support, the CEDAR-H project is progressing and will be commissioned on the H6 line in a testbeam in Autumn 2022. Given the benefit to the experiment, CEDAR-H will be installed as soon as the new system is fully validated with testbeam data. Once this is done the existing CEDAR-W filled with nitrogen will be available as a fully operational spare to mitigate the risk of relying on such a unique instrument.

3.1.1 GTK

The GigaTracker beam spectrometer is critical for the $K^+ \rightarrow \pi^+ \nu \bar{\nu}$ analysis strategy: it must efficiently and precisely reconstruct beam K^+ tracks to provide a momentum and direction measurement, and allow matching with downstream tracks.

The hits produced by the GTK detector are sent to the readout boards, where they are matched in time with the triggers provided by the L0 Trigger Processor (L0TP). The hits are organized in 6.4 μs frames, each made by 16 time windows of 400 ns. The trigger matching procedure selects hits belonging to the same window (hence, to the same frame). An inefficiency of about 5% was observed in 2021 due to the presence of the trigger at the edges of a 400 ns window, and work is on-going to reduce it. An additional inefficiency was observed in 2018 data due to a limit in the firmware on the number of hits per half-chip in each frame, that becomes higher when the intensity increases. This was the dominant source of GTK-DAQ inefficiency in 2018, reaching about 10% at nominal intensity. In 2021 data taking, the limit on the number of hits has been increased, successfully making the inefficiency negligible.

Besides DAQ inefficiency, in 2021 the GTK system experienced periods of instability in all the stations except for GTK3. During these periods, the synchronization between the readout chips and the boards (located in different zones of the experimental area) was lost and the hits were not correctly processed by the boards. The source of the instabilities seems to be a large component of beam halo that causes Single-Event-Upsets (SEUs) reaching the PCB of GTK stations 0, 1 and 2, while GTK3 is shielded by the presence of the sweeper and Trim 5 (in 2018 GTK2 and GTK3 were in the shielded position). This observation has been confirmed

by comparing the number of SEUs reported by CERN radiation monitors close to GTK1 and GTK3 printed circuit boards (PCBs); an independent measurement of the beam halo and its distribution during the spills has been obtained with scintillating tiles installed close to GTK1 electronics.

After the end of 2021 data taking, both firmware and DAQ software were updated in order to increase the synchronization stability and to reduce the time to recover from error states due to SEUs. Improved beam steering and focusing in NA62 will be mandatory in 2022. Radiation monitors installed close to each GTK station will also improve the control of the area surrounding the beam pipe, where sensitive electronics can be affected by an increase in the halo.

Since last report, three new GTK modules have been produced while the remaining ones will be delivered in the next months; according to the current schedule, the production of GTK detectors should be completed by June 2023.

3.2 Trigger, DAQ and Operation

The work on the Data Acquisition (detector readouts, PCFarm, RunControl) was concentrated on adding new detectors (GTK0, Anti0, VetoCounter, HASC2), and in finding solutions or mitigation for the issues observed during the 2018 test at high beam intensity. Several studies have been made to improve and optimise the trigger system, particularly considering the challenge of increased beam intensity.

The work on the GTK readout has been summarised above. Regular interactions with the company CAEN (author of the CREAM readout firmware) are on-going, in order to solve some features of the LKr calorimeter readout seen during previous data taking periods. The main aims were to eliminate the “swap” issue (where the values of the first 16 channels were swapped with the other 16) at initialization, and to fix an issue in the multi-event packing (implemented to reduce the number of packets on the network) where a sizeable number of packets are sent to the wrong farm PCs. A version of the LKr readout firmware solving the “swap” problem was prepared and deployed for the 2021 run with good performance, and no issues were observed after the initialization of the modules. The readout performed well in 2021 up to 1 MHz L0 trigger rate. The work by CAEN is still on-going to fix the misbehavior of the readout data packing mode; the solution could help reduce the number of data packets travelling on the network.

New CFD modules for the VetoCounter are being prepared and will be operational for the 2022 run. The new prototype FPGA-based TDC system (higher rate, no dead time), read out by the ATLAS FELIX PCIe board installed into a server, was installed for the new VetoCounter and tested at the end of the run. Given its performance at high rate, the system is potentially useful for the highest-rate detectors like KTAG and CHANTI: a complete new TDC system has been prepared to be used in a test run with the CHANTI front-end electronics in parallel with the default acquisition. An useful feature of the FELIX system is that the complete spill data is available in memory. Moreover a fast spill shape report with a time granularity of 800 ns can be generated as a by-product of the hit sorting algorithm.

The CHOKE is a warning signal sent by detectors when their buffers are almost full; it is detected by the L0TP, that then stops dispatching triggers until the critical period has ended. The importance of using the CHOKE lines was already demonstrated in 2018, albeit with only a few detectors connected. The CHOKE mechanism was activated in 2021 for all the detectors with a CHOKE line. Problems of noise on the CHOKE line, possibly due to pumps or magnets in the area, have been partially addressed in 2021 and will be fully addressed in 2022.

Supercell time corrections were introduced in the LKr L0 trigger, improving its time resolution. The installation in the L0 calorimeter trigger system of a dedicated readout to output the energy and position of the clusters has been delayed due to the pandemic. The aim is to

incorporate it in the High-Level-Trigger algorithms in the 2022 data taking after commissioning. Minor modifications to L0 trigger conditions were made, increasing the requirements on the number of hits in RICH and NewCHOD and the number of clusters in LKr, to tighten the selection while maintaining high efficiency.

The main development in the High-Level Trigger (HLT) has been the creation of an online framework that reproduces the PCFarm online environment. This is ideal for debugging of new algorithms, and also for simulating the multi-threading environment and the L1 data packet distribution flow. This online framework is additional to the already existing offline framework, integrated into the official data reconstruction environment, that is more suitable to re-execute algorithms on data and compute trigger efficiencies. On the algorithm side, several new algorithms have been devised, using information from the MUV3, LAV and STRAW detectors. In particular, online STRAW track reconstruction can select different event categories such as $\pi^+\nu\bar{\nu}$, one-track final states, multi-track (di-electron, di-muon) final states, or even perform a rough calculation of the squared missing mass. The efficiency and reduction factors of all new HLT algorithms have been studied offline in a preliminary way during 2021 data taking; all performances will be re-assessed with the reprocessed data. The best conditions in terms of high efficiency and high reduction factor will be deployed online in 2022.

The oscillations in the number of L0 triggers from burst to burst, seen in 2018 in a test at nominal beam intensity, were understood in 2021 as originating from the Ethernet switches used to duplicate the flow of the trigger primitives to be sent to the primitive acquisition. The problem was identified in the poor latency behavior of the switch used. A temporary solution removing the switches, therefore losing the primitive duplication, was implemented in 2021. A permanent solution has been identified, in the use of Ethernet TAPs, able to mirror an Ethernet flow with basically zero latency. A set of Ethernet TAP has been installed and it will be used in 2022. The replacement of the L0TP (L0TP+) based on a more modern technology is planned during Run2. Preliminary checks have been done in the Laboratory and in the experiment (signal receiving etc.). The new system will initially run in parallel with the standard L0TP. As soon as the firmware is complete, the system will be validated with beam, making use of the new Ethernet TAP system. Due to the switch problem mentioned above during 2021, it was only possible to monitor one channel of primitives and the commissioning could not be concluded.

The Run Control of the experiment has been upgraded with the addition of the new detectors. In addition, a new subsystem for the monitor of the trigger and DAQ efficiency, based on data collected by various subsystems and presented in a series of plots and tables, was tested in 2021, and will be used systematically in 2022 to monitor daily efficiency. As an example, the monitor system recorded a T4 beam time availability of about 70% that is compatible with the official number distributed by beam operation, and a T10 beam time availability of about 87%, that includes the beam setup issues observed at the start of the 2021 data taking period. The sources of down-time for NA62 itself are being examined and are largely dominated by problems related to the beam intensity being much larger than nominal at the start of the spill, as described in Section 2. The NA62 Online Monitor, rewritten using the NA62 Analysis framework to have multi-layer feedback, will be tuned for enhanced performance in 2022 (Section 4).

In 2021 a series of actions were taken in order to be able to operate the experiment even in case of stringent restrictions due to Covid-19. In particular, we requested in-person shifters to group their presence at CERN to minimize travel and its covid-related risks; also the role of general expert was introduced, to help the Run Coordinator to handle problems when experts were acting remotely. For this interaction with the remote experts we installed a dedicated camera in the control room, able to focus on all the screens, and an audio station for zoom connections. Luckily, the international situation was not very problematic during the 2021 data taking period, and these additional measures were only occasionally used. However, at the beginning of October, we had to take data for about two weeks in an emergency mode with

only the Run Coordinator and one shifter in the control room, while the second one was remote. Although the pandemic situation seems to be improving, we will refine our rules to be prepared for similar circumstances in 2022.

4 Data quality and data processing

The full reprocessing of 2021 data with the most recent reconstruction software version started in February 2022, and will be completed before the 2022 data taking starts.

During 2021, most of the effort was concentrated on including the reconstruction and data quality assessment for the detectors newly installed for the 2021 data taking, namely the Veto-Counter, ANTI0, the additional station of GTK, and the second module of the HASC. Moreover, we continued to improve the calibration procedure and the reconstruction algorithms of several Run1 detectors, to improve their performance at higher beam intensities.

In the GTK, tracks are reconstructed using a 4D technique, where the XY information from the silicon pixels is combined with the Z coordinate of the station and with the hit times thanks to the excellent (~ 140 ps) time resolution. The reconstruction software has been updated in order to handle the hits from the additional GTK0 and the code has been optimized using a two-steps algorithm: in the first step the hits in each station are sorted by time, then groups from different stations are clusterized in time and space. The optimization of the algorithm substantially reduced the CPU time spent by GTK reconstruction for each event.

The reconstruction software of the LKr calorimeter, a legacy from NA48 and still partially written in FORTRAN, was converted and re-written within the C++ framework, vastly improving on some features. In particular, the algorithm is now much less intensity dependent and has better handling of the pileup. The improvements were fully tested and committed during 2021. All analyses benefit from the new LKr reconstruction with reconstruction efficiency improving by up to 10% depending on the analysis. The impact is particularly evident in the $K^+ \rightarrow \pi^+ \nu \bar{\nu}$ analysis (see Section 6). In addition, a new energy calibration using photons from π^0 Dalitz decays was fully implemented.

A new Online Monitor system, based on multi-layer feedback (online/fast/prompt) was implemented in view of the 2021 data taking:

Online: fast feedback, low-level quality checks (e.g. detector occupancies), in order to alert data-taking shifters to take immediate actions.

Fast: high-level quality checks (e.g. detector efficiencies), in order to provide feedback on the sub-detector performances to the sub-detector experts.

Prompt: full reprocessing of the collected data, including all the automatic calibration procedures, in order to allow analysts to perform their analysis on the newly collected data.

A consequence of the especially-high-intensity first second of the spill (see Section 2) was that the Online Monitor processing time was higher than expected: the online feedback was available a few minutes after the burst was collected, while in 2018 it was usually taking a few tens of seconds. We are currently investigating methods to speed the processing up for the 2022 data taking, including the redesign of the NA62 reconstruction core to allow multi-threading and the direct transmission of single events from the PC farm nodes to the monitor machines via network, to bypass the raw file building by the mergers and reduce the I/O transfer time.

Another consequence of the spill problem was the increased data size in every spill, nearly double compared to 2018, which might affect our processing and data storage requirements should this problem persist for 2022 and later. The estimate of the expected data rates and resources needed for the 2021–25 data taking was based originally on the 2018 data, as a similar

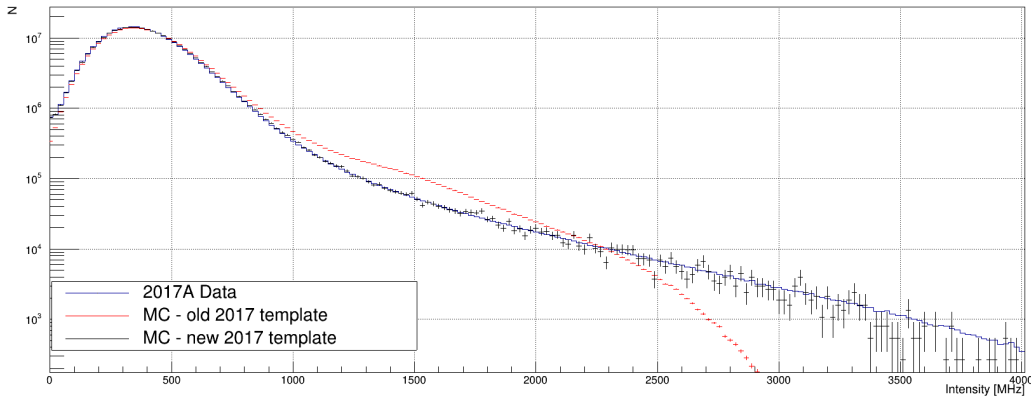


Figure 5: Number of events (arbitrary units) as a function of the intensity (MHz) measured from the GTK time sidebands, with previous (red) and current (black) Monte Carlo intensity template, compared with 2017 data (blue).

rate of raw data was expected. If we are able to mitigate the problem of the first second of the spill in 2022, the projection is still valid: a total of about 15 PByte of CTA space by the end of 2025. For EOS, about 10 PByte of space is expected to be needed to perform analyses by 2025, with a steady increase of about 1 PByte during each year of data taking. All the projections into the future are subject to uncertainties, and can and will be refined as time goes on, in particular after the number of days of allocated beam time in every single year is known, and the outcome of the spill shape problem is known.

We would like to express our gratitude to the IT Department for their support and expertise in assisting the needs of the experiment, and in particular to Xavier Espinal and Bernd Panzer-Steindel, for the excellent support and services provided to us.

5 MC validation

Several important improvements to the NA62 MC simulation software have been implemented in the last year.

A more accurate simulation of the accidental activity was achieved thanks to a new strategy to obtain the true beam intensity employing Bayesian unfolding with the RooUnfold [4] framework. The distribution of instantaneous intensity, from the Monte Carlo simulation of 2017 conditions, obtained with the previous and current technique is shown in Fig. 5, compared with the one from 2017 data. Moreover, the possibility to force specific accidental coincidences was introduced, in order to reproduce rare background mechanisms leading to multiple event coincidences. The main use-case of this new biased overlay technique is currently an ongoing five-track analysis, in which several overlapping three-track decays can be interpreted as the signal.

The NA62 MC simulation code was extensively modified, in order to move all the beam optics and detector geometry definitions in a dedicated configuration file and allow a more flexible choice of the simulated layout. Abstract parsing and factory classes were introduced to read such information and create the beam line elements, while taking care of geometry overlaps automatically. In addition, detector geometries, which contained many distributed elements, were re-factored to allow for individual placement based on the configuration file. This work will also allow sensitivity studies of future beam line configurations for high-intensity kaon experiments with K^+ and K_L beams, that the collaboration is planning.

Finally, the MC true hit merging and hit information was propagated up to the analysis

level, which will facilitate the backtracking and debugging of pathological background events.

6 Status of the $K^+ \rightarrow \pi^+ \nu \bar{\nu}$ analysis

The theoretical prediction of the $K^+ \rightarrow \pi^+ \nu \bar{\nu}$ decay branching ratio is subject only to a small uncertainty [5, 6, 7, 8, 9, 10]. This decay is among the most promising modes to search for non-Standard-Model signals in flavour physics, as it probes higher mass scales than other rare meson decays, and several models foresee deviations from Standard Model predictions [11, 12, 13, 14, 15, 16, 17, 18, 19, 20].

Data taken in 2018 have been fully analysed, and the final result, including the combination of the results from the 2016 and 2017 analysis has been published [3]. The branching ratio, measured with the full 2016–2018 (Run1) dataset, is

$$\mathcal{B}(K^+ \rightarrow \pi^+ \nu \bar{\nu}) = (10.6_{-3.4}^{+4.0})_{\text{stat}} \pm 0.9_{\text{syst}} \times 10^{-11} \quad \text{at 68\% CL.} \quad (1)$$

The result is the most precise determination of the $K^+ \rightarrow \pi^+ \nu \bar{\nu}$ decay rate to date and provides the strongest evidence so far for the existence of this process.

6.1 Run 2 analysis and increased intensities

The next phase of the analysis, towards improved precision, is underway using new data collected in 2021 with higher beam intensities [21]. The number of particles delivered by the SPS per burst, as measured by the T10 and ArgonIon counters, was increased to, and maintained at, approximately 100% of the nominal NA62 specification from early September. The experiment successfully took data in these conditions, fulfilling an important target for the 2021 data-taking.

In events with instantaneous intensity significantly above the nominal design rate, high numbers of signals in the detector systems (high multiplicity) is observed. The selection of $K^+ \rightarrow \pi^+ \nu \bar{\nu}$ candidates relies on stringent and hermetic veto requirements which reject high multiplicity events. Therefore, during the early part of spill the efficiency for the study of the $K^+ \rightarrow \pi^+ \nu \bar{\nu}$ decay is degraded. The distribution of the instantaneous intensity for selected normalisation $K^+ \rightarrow \pi^+ \pi^0$ events, measured using the number of hits in time sidebands in the GTK beam spectrometer, is shown in Fig. 6 (left), comparing 2018 and 2021 data. The average instantaneous intensity for selected normalisation events has increased by approximately 30%, in relative terms, with respect to 2018. This is less than the measured increase in total particles per spill because of the highly non-flat spill structure, and the fact that the trigger and selection preferentially selects events away from the instantaneous intensity peaks (see Section 2).

With the increase in intensity it has been imperative to re-optimize the veto criteria to prevent excessive rejection of events due to random activity. This is quantified by the random veto efficiency, ε_{RV} , which measures the fraction of events passing photon and multiplicity veto criteria applied only in the signal selection. Fig. 6 (right) shows a comparison of ε_{RV} as a function of instantaneous beam intensity for 2018 and 2021 data and selections. Improvements to the selection have led to important increases in ε_{RV} . A noteworthy example is that improvements in the LKr reconstruction meant that the time windows for the LKr photon veto could be reduced significantly, with the effect that the signal efficiency after photon rejection increased by about 10% compared to the old reconstruction. These improvements have meant that despite the increased average intensity, the overall random veto efficiency remained almost stable within uncertainty with respect to 2018:

$$\varepsilon_{RV}^{2018} = (66 \pm 1)\%, \quad \varepsilon_{RV}^{2021} = (64 \pm 2)\%.$$

Further work towards improving this is ongoing.

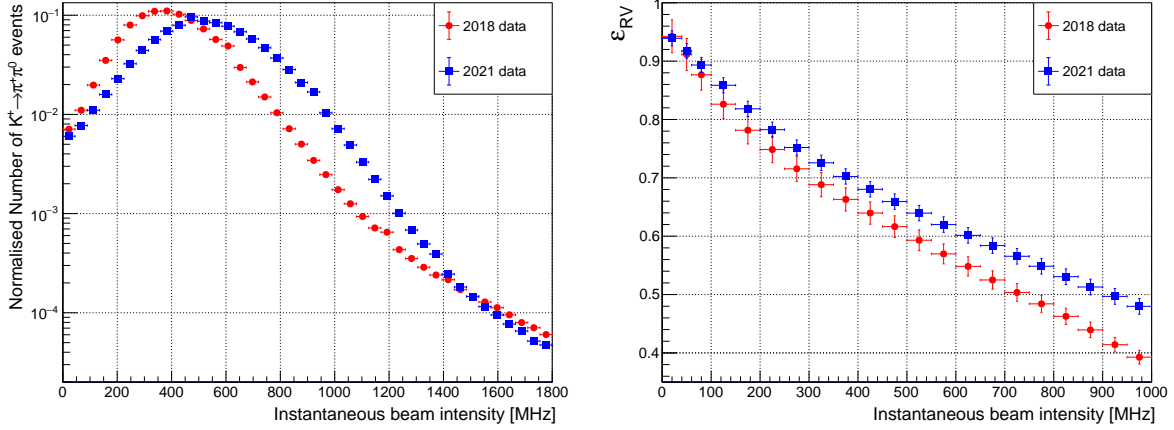


Figure 6: Normalised distributions of numbers of normalisation $K^+ \rightarrow \pi^+\pi^0$ events (left) and random veto efficiency, ε_{RV} , (right), as functions of instantaneous beam intensity for representative sub-sets of 2018 and 2021 data.

6.2 New detector systems

In 2021 three new detectors were installed, designed to further enhance the $K^+ \rightarrow \pi^+\nu\bar{\nu}$ analysis, these are: a fourth GTK station, the VetoCounter and the HASC2.

The GigaTracker beam spectrometer (GTK) is critical for the $K^+ \rightarrow \pi^+\nu\bar{\nu}$ analysis strategy. The addition of a fourth GTK station provides extra information which can be exploited to more effectively and efficiently reject upstream background and improve kaon-pion matching performance. In the Run 1 analysis events were rejected with additional in-time GTK hits not associated to a selected kaon GTK track, and this criteria was effective in suppressing upstream background. With the new GTK station additional station pair or triplet correlations can be exploited to further improve this procedure. Several options for improving the kaon-pion matching algorithm are under study, including machine learning approaches where additional station-specific information can help improve overall performance.

Upstream $K^+ \rightarrow \pi^+\pi^0$ and $K^+ \rightarrow \pi^+\pi^+\pi^-$ decays are responsible for the principal upstream backgrounds for the $K^+ \rightarrow \pi^+\nu\bar{\nu}$ analysis; π^\pm are primarily detected in VC1 while photons from $\pi^0 \rightarrow \gamma\gamma$ are detected in VC2 after electromagnetic showers are instigated in the lead sheet. Halo muons can traverse all three VetoCounter stations and, since they are efficiently rejected by other components of the $K^+ \rightarrow \pi^+\nu\bar{\nu}$ selection, events with coincident signals in all three VetoCounters will not be specifically rejected. Therefore, by correlating signals in the three planes a simple particle identification can be performed that can allow specific restrictive veto criteria to be applied to suppress upstream backgrounds without introducing inefficiency from vetoing due to random activity.

The reduced efficiency of the VetoCounter detector in 2021 means the impact on the upstream background will not be as significant as when the system is fully optimised in 2022. Nevertheless, studies are ongoing on the usage of the VetoCounter in the $K^+ \rightarrow \pi^+\nu\bar{\nu}$ selection and initial results achieve a suppression of upstream-like events by a factor of 2, with rejection of only 3% due to random activity. This is based on a conservative veto criteria rejecting associated VetoCounter candidates within 2 ns of the KTAG K^+ reference time and was assessed based on control samples selected in data, as shown in Fig. 7 (left). In 2022 new CFDs will be used and the system will be optimised, increasing the efficiency of the VetoCounter and allowing further rejection power, which is key to reduce the primary background for to the $K^+ \rightarrow \pi^+\nu\bar{\nu}$ analysis.

Analysis of 2016-2018 data demonstrated that the HASC can be used to reject photons from π^0 decays, in addition to the original design concept that suppresses $K^+ \rightarrow \pi^+\pi^+\pi^-$ decays

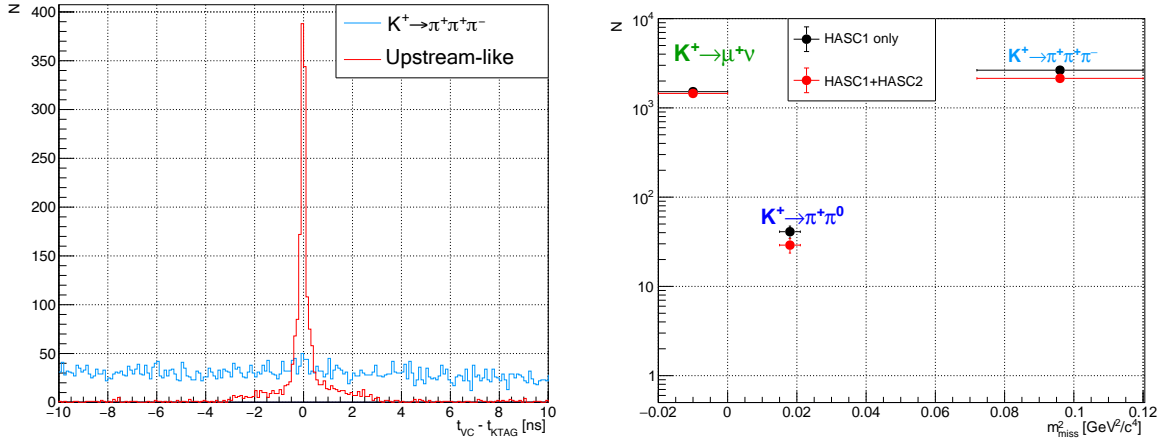


Figure 7: Left: time difference between VetoCounter candidates and the KTAG reference time ($t_{VC} - t_{KTAG}$) for two control samples labeled $K^+ \rightarrow \pi^+\pi^+\pi^-$ and upstream-like. The former shows only random activity in the VetoCounter since the K^+ projected position is required to be consistent with the beam and therefore outside the VetoCounter. Conversely the latter shows in-time activity in the VetoCounter associated with upstream-like events selected by inverting upstream rejection cuts in the $\pi\nu\bar{\nu}$ selection. Right: numbers of events passing the $\pi\nu\bar{\nu}$ selection in 2021 data, in three control regions dominated by $K^+ \rightarrow \mu^+\nu$, $K^+ \rightarrow \pi^+\pi^0$ and $K^+ \rightarrow \pi^+\pi^+\pi^-$ decays (as labeled), with the HASC1 only or both HASC stations used in the $\pi\nu\bar{\nu}$ selection (see text for quantitative details).

through detection of high-momentum π^+ . Analysis of 2021 data has demonstrated that the addition of HASC2 further suppresses the $K^+ \rightarrow \pi^+\pi^0$ and $K^+ \rightarrow \pi^+\pi^+\pi^-$ backgrounds by 35% and 19% respectively, as shown by Fig. 7 (right), without a noticeable increase in random veto. Importantly, this means that the $K^+ \rightarrow \pi^+\pi^0$ background, formerly the second largest [3], is suppressed to a similar level to the $K^+ \rightarrow \mu^+\nu_\mu$ decay.

The inclusion of new detector systems is having a significant positive impact on the $K^+ \rightarrow \pi^+\nu\bar{\nu}$ analysis, with suppression of the two largest backgrounds already demonstrated. Further studies are ongoing to fully exploit the additional information provided by the new detectors.

6.3 Next steps

The processing of the full 2021 data set is currently ongoing, including the full set of calibrations and enhanced quality control. Once completed, the performance of the $K^+ \rightarrow \pi^+\nu\bar{\nu}$ analysis, the sensitivity and backgrounds, will be quantified in detail. Simultaneously, improvements on the analysis strategies are under development. This includes using machine learning techniques for particle identification and matching upstream and downstream tracks, and completing the re-optimisation of the analysis for higher intensities.

The 2021 data set is limited in size, and is expected to be no larger than 35% of the 2018 data set, due to the reduced number of days (beam availability), and the beam spill quality and related inefficiencies.

Preparations for 2022 data taking have been put in place, including development of a system for fast feedback of key performance indicators from the $K^+ \rightarrow \pi^+\nu\bar{\nu}$ analysis, such as the random veto efficiency. This information will be provided to the data-taking teams to help identify issues promptly and provide a preliminary assessment of the quality of data. This supplements the suite of tools available in previous years, which generally concentrate on more low-level and detector-specific performance indicators.

7 Rare and forbidden decays

The rare decay physics programme is enabled by the auxiliary prescaled multi-track trigger chains operating along with the main $K^+ \rightarrow \pi^+ \nu \bar{\nu}$ trigger. The L0 triggers for collection of K^+ decays to lepton pairs are based on RICH and CHOD multiplicity requirements, as well as the total LKr energy deposit and MUV3 signal multiplicity conditions. The L1 trigger involves beam kaon identification by the KTAG and fast reconstruction of a negatively charged track in the STRAW spectrometer. The dataset collected in 2016–18 is equivalent to 3×10^{12} kaon decays in the vacuum tank to di-muons, 10^{12} decays to di-electrons, and 10^{12} decays to electron-muon pairs. Datasets collected with generic multi-track and minimum bias trigger conditions are equivalent to about 10^{11} kaon decays in total.

Following a detailed trigger purity and efficiency analysis with the 2016–18 data and simulations, the multi-track trigger chains have been optimised for data collection at higher beam intensity in 2021. Improvements to the L0 CHOD and the RICH multiplicity conditions have led to a reduction of the multi-track trigger rates by about a factor of two, with trigger efficiency reduction by 3% with respect to the 2016–18 conditions (to about 95% for the $K^+ \rightarrow \pi^+ \pi^+ \pi^-$ decay). A planned update of the L0 calorimeter trigger based on cluster topology information is expected to bring further improvement (by an estimated 20%) in the di-electron trigger purity. Optimisation of the fast STRAW track reconstruction algorithm has improved the L1 multi-track efficiency by 3% with respect to the 2016–18 data taking (to about 97% for the $K^+ \rightarrow \pi^+ e^+ e^-$ decay). A new L1 di-electron trigger algorithm using both the STRAW and RICH information has been developed for deployment in 2022, and is expected to reduce the di-electron trigger rate by a further 70%, with an estimated 2% reduction in efficiency for the $K^+ \rightarrow \pi^+ e^+ e^-$ decay. These improvements are expected to allow a significant reduction of the trigger downscaling factors, despite operation at higher beam intensity than in 2016–18.

The problematic SPS beam spill intensity profile in 2021 has inhibited the full exploitation of the improved trigger chains. As a result, the 2021 rare decay dataset is significantly smaller than the 2016–18 one. This dataset is nevertheless important for the further development of the trigger and physics analysis techniques.

The collaboration has presented a new preliminary measurement of the radiative $K^+ \rightarrow \pi^0 e^+ \nu \gamma$ ($K_{e3\gamma}$) decay with the 2017–18 dataset at the EPS-HEP conference in 2021 [22]. The ratio of the branching fractions for $K^+ \rightarrow \pi^0 e^+ \nu \gamma$ and $K^+ \rightarrow \pi^0 e^+ \nu$ (K_{e3}) is measured using the minimum bias dataset in three $K_{e3\gamma}$ kinematic regions defined by the photon energy, E_γ , and the angle between the positron and the photon, $\theta_{e\gamma}$, in the kaon rest frame. The results summarised in Table 1 improve on the previous measurements [23, 24] by factors between 2.0 and 3.6, and are in 6–7% disagreement with the chiral perturbation theory (ChPT) $O(p^6)$ expectation [25]. A signal missing mass spectrum obtained in one of the kinematic regions (R1) is displayed in Fig. 8.

A comprehensive programme of searches for lepton number and lepton flavour violating K^+ decays with the 2016–18 dataset has been mostly completed. The following upper limits at 90% CL of the decay branching fractions have been reported in three papers, two of which were published in the last year [26, 27, 28]:

$$\begin{aligned}
 \mathcal{B}(K^+ \rightarrow \pi^- e^+ e^+) &< 5.3 \times 10^{-11}, \\
 \mathcal{B}(K^+ \rightarrow \pi^- \pi^0 e^+ e^+) &< 8.5 \times 10^{-10}, \\
 \mathcal{B}(K^+ \rightarrow \pi^- \mu^+ \mu^+) &< 4.2 \times 10^{-11}, \\
 \mathcal{B}(K^+ \rightarrow \pi^- \mu^+ e^+) &< 4.2 \times 10^{-11}, \\
 \mathcal{B}(K^+ \rightarrow \pi^+ \mu^- e^+) &< 6.6 \times 10^{-11}, \\
 \mathcal{B}(\pi^0 \rightarrow \mu^- e^+) &< 3.2 \times 10^{-10}.
 \end{aligned}$$

Table 1: Definitions of the ratios $R_i = \mathcal{B}(K_{e3\gamma}^i)/\mathcal{B}(K_{e3})$ in terms of E_γ and $\theta_{e\gamma}$, ChPT $O(p^6)$ expectations for these ratios [25], and preliminary NA62 measurements of these ratios [22].

	E_γ^i	$\theta_{e\gamma}^i$	ChPT $O(p^6)$	NA62 (preliminary)
$R_1 \times 10^2$	$E_\gamma > 10$ MeV	$\theta_{e\gamma} > 10^\circ$	1.804 ± 0.021	$1.684 \pm 0.005 \pm 0.010$
$R_2 \times 10^2$	$E_\gamma > 30$ MeV	$\theta_{e\gamma} > 20^\circ$	0.640 ± 0.008	$0.599 \pm 0.003 \pm 0.005$
$R_3 \times 10^2$	$E_\gamma > 10$ MeV	$0.6 < \cos \theta_{e\gamma} < 0.9$	0.559 ± 0.006	$0.523 \pm 0.003 \pm 0.003$

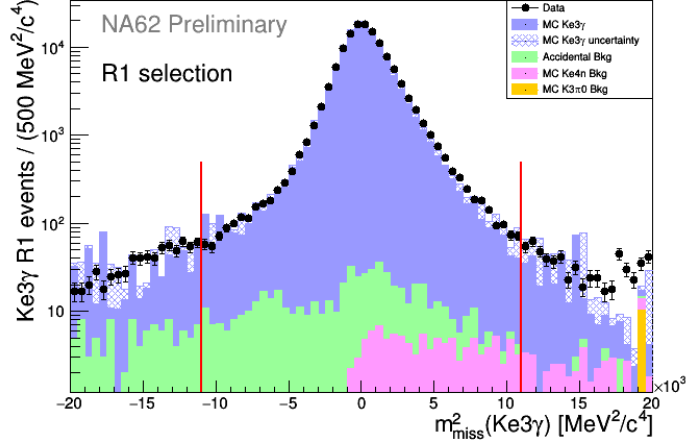


Figure 8: Reconstructed squared missing mass spectrum obtained within the analysis of the radiative $K_{e3\gamma}$ decay based on the 2017–2018 data [22].

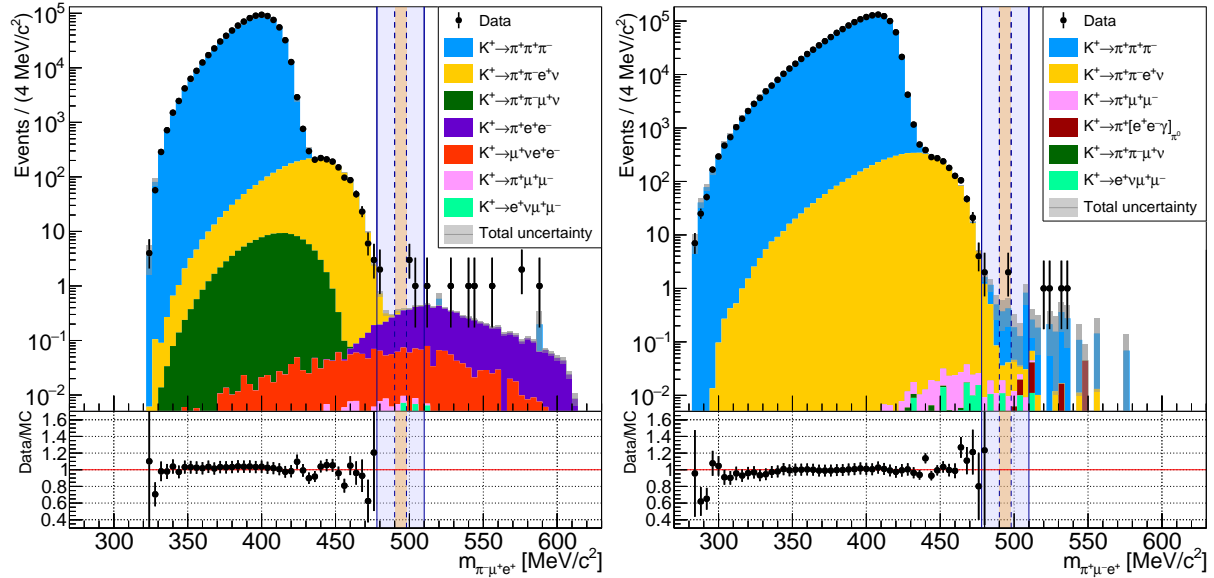


Figure 9: Reconstructed mass spectra, and data/MC ratios, obtained in the searches for the forbidden $K^+ \rightarrow \pi^- \mu^+ e^+$ (left) and $K^+ \rightarrow \pi^+ \mu^- e^+$ (right) decays based on the 2016–2018 data [27].

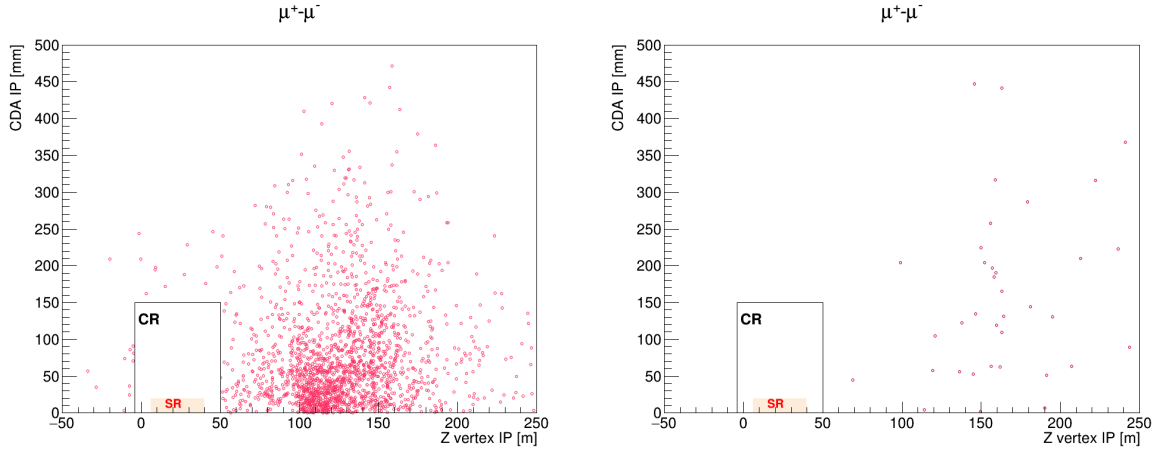


Figure 10: Selected events with candidate $\mu^+\mu^-$ vertices. Closest distance of approach of the total di-muon momentum to the proton beam impact point as a function of the longitudinal position of the minimum approach along the beam axis. The region close to the tax is blinded as this is the region of expected origin of signal events. Left-hand side: data from the 2017/2018 period corresponding to about 2.6×10^{16} protons on tax (POT). Right-hand side: data from the 2021 data-taking corresponding to about 1.3×10^{17} POT. Despite the larger statistics in 2021, the di-muon background is reduced by more than 2 orders of magnitude.

As an illustration, reconstructed missing mass spectra obtained within the searches for the $K^+ \rightarrow \pi^\pm \mu^\mp e^+$ decays are shown in Fig. 9.

Searches for heavy neutral lepton (N) production in $K^+ \rightarrow e^+ N$ and $K^+ \rightarrow \mu^+ N$ decays and for the $K^+ \rightarrow \mu^+ \nu X_{\text{inv}}$ decays with the full 2016–18 dataset have been completed [29, 30]. These results, along with the recently published $K^+ \rightarrow \pi^+ X_{\text{inv}}$ searches with the full dataset [3, 31], represent the first steps in a comprehensive programme of searches for hidden sectors in K^+ decays at NA62. The roadmap for hidden-sector searches in kaon decays has been established in a recent review paper with strong engagement from the NA62 collaboration [32].

8 Exotic processes

In October 2021, approximately one week of data was taken in the so-called beam-dump mode. During this period, the intensity of the proton beam dumped on the TAX was above 150% of the NA62 nominal intensity. Thanks to a careful optimisation of the T4-to-T10 beam transmission efficiency by the beam division personnel, no problems in terms of radio-protection limited the data taking. The total accumulated statistics exceeds 10^{17} POT.

The 2021 data taking was carried out with optimized settings for muon sweeping as proposed in studies carried out in the context of the Physics Beyond Colliders (PBC) initiative at CERN [33]. The magnets of the upstream achromat were re-cabled to allow an independent current setting for the two dipoles just downstream of the TAX. While during the ‘standard’ NA62 data-taking, these dipoles are set to have opposite currents and maximum strength, simulations [33] suggested an optimal sweeping if same-sign currents were set, with the first magnet downstream of the TAX at the maximum strength and the other at approximately one third of the maximum. In these conditions, a factor of 4 overall muon flux reduction was expected (cf. Fig. 11). The data taking fully confirmed the simulation estimates: during the commissioning of the beam for the dump mode, a wide scan on the second dipole after the TAX was performed observing the muon rates, which confirmed the simulation. In addition to the reduction of the flux of single muons, the beam line setup used allows an effective sweeping of particles from the

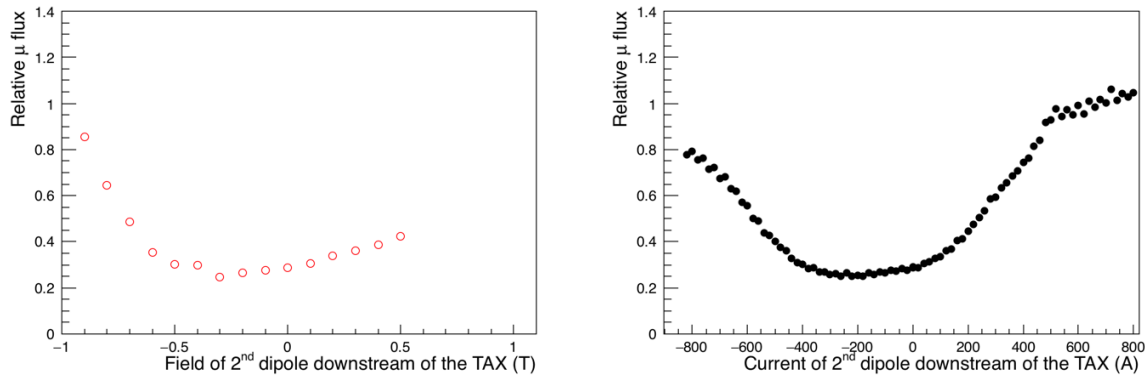


Figure 11: Muon rate normalized to the rate in nominal data-taking as a function of the setup of the second dipole downstream of the TAX. Monte Carlo expectation as a function of the dipole field (left panel) and data measurement as a function of the dipole current (right panel). The flux can be reduced by a factor of four.

TAX with momentum above about 15 GeV, that turns out to be instrumental for background reduction.

In addition to the beamline optimization, triggers were optimized on the basis of the experience gathered with 2017/2018 data. As described in the 2021 SPSC report, past beam dump data was affected by a problem that penalized the most the trigger line with the lowest rate, which was the neutral trigger line. As a result, the average efficiency of that trigger line was only 40%. The L0 firmware mechanisms responsible for it was fully understood and modelled, and at the beginning of 2019, the firmware was corrected for future data taking. As a result, in 2021 the trigger efficiency of the neutral trigger line is above 98% for calorimeter energy deposits above 5 GeV. In addition, in 2021 the charged trigger has been upgraded. A two-particle trigger requiring at least two, mutually in-time, energy releases in the CHOD has been implemented. This is more inclusive for exotic particle decays close to the kinematic threshold than the condition used for 2017–18 beam dump data (energy releases in at least two CHOD quadrants). The efficiency of the charged trigger exceeds 98%.

The data taken in 2021 is currently being analysed and preliminary results, also shown at the PBC general meeting [34], reveal an encouraging prospect for exotics searches. As an example, the prospects for the search of ALPs decaying to two muons [35] are promising: despite a factor of ~ 20 higher statistics in terms of dumped protons compared to the data taken in 2017–18, the number of events outside the signal region is reduced by a factor of ~ 10 in absolute terms, corresponding to an overall background reduction of ~ 200 (cf. Fig. 10). The new ANTI0 detector has been seen to reduce the background by a further factor of ten: in Figure 10 (right) the ANTI0 is not used to preserve the possibility to compare with previous data. For di-photon final states, in a preliminary analysis a background reduction of about a factor 20 has been observed outside the signal region.

9 Publication of NA62 results

Since the last NA62 SPSC review in April 2021, the collaboration has completed the following publications:

- E. Cortina Gil et al. (NA62 collab.), Searches for lepton number violating $K^+ \rightarrow \pi^-(\pi^0)e^+e^+$ decays, arXiv:2202.00331, submitted to Physics Letters B [28].

- E. Cortina Gil et al. (NA62 collab.), Search for lepton number and flavour violation in K^+ and π^0 decays, Physics Review Letters, Volume 127, 131802 (2021) [27].
- E. Cortina Gil et al. (NA62 collab.), Measurement of the very rare $K^+ \rightarrow \pi^+ \nu \bar{\nu}$ decay, Journal of High Energy Physics, Volume 2021, Issue 6, page 93 [3].
- E. Cortina Gil et al. (NA62 collab.), Search for K^+ decays to a muon and invisible particles, Physics Letters B 816 (2021) 136259 [30].

The collaboration is actively contributing to major International Conferences and topical Workshops with recently published or preliminary physics results from NA62 and NA48/2 data analyses. In the past year (May 2021 to April 2022), collaboration speakers presented 21 plenary talks and 36 parallel talks. Although several conferences were held online, the number of contributions is compatible with the pre-covid average. In particular, NA62 contributed several results and presentations to the EPS-HEP 2021 and Lepton Photon 2021 Conferences. More contributions are already foreseen in future 2022 Conferences.

References

- [1] 2021 NA62 Status Report to the CERN, SPSC-SR-286.
- [2] E. Cortina Gil *et al.* (NA62 collab.), JINST **12** (2017) P05025.
- [3] E. Cortina Gil *et al.* (NA62 collab.), JHEP **06** (2021) 093.
- [4] Tim Adye, Proceedings of the PHYSTAT 2011 Workshop on Statistical Issues Related to Discovery Claims in Search Experiments and Unfolding, CERN, Geneva, Switzerland, 17–20 January 2011, edited by H.B. Prosper and L. Lyons, CERN–2011–006, pp. 313–318.
- [5] A.J. Buras, D. Buttazzo, J. Girrbach-Noe and R. Knegjens, JHEP **11** (2015) 33.
- [6] G. Buchalla and A.J. Buras, Nucl. Phys. **B548** (1999) 309.
- [7] A.J. Buras, M. Gorbahn, U. Haisch and U. Nierste, Phys. Rev. Lett. **95** (2005) 261805.
- [8] J. Brod, M. Gorbahn and E. Stamou, Phys. Rev. **D83** (2011) 034030.
- [9] G. Isidori, F. Mescia and C. Smith, Nucl. Phys. **B718** (2005) 319.
- [10] F. Mescia and C. Smith, Phys. Rev. **D76** (2007) 034017.
- [11] M. Blanke, A.J. Buras and S. Recksiegel, Eur. Phys. J. **C76** (2016) 182.
- [12] M. Blanke, A.J. Buras, B. Duling, K. Gemmler and S. Gori, JHEP **03** (2009) 108.
- [13] A.J. Buras, D. Buttazzo and R. Knegjens, JHEP **11** (2015) 166.
- [14] J. Aebischer, A.J. Buras and J. Kumar, JHEP **12** (2020) 097.
- [15] G. Isidori, F. Mescia, P. Paradisi, C. Smith and S. Trine, JHEP **08** (2006) 064.
- [16] M. Tanimoto and K. Yamamoto, Prog. Theor. Exp. Phys. **2016** 123B02 (2016).
- [17] T. Blazek and P. Matak, Int. J. Mod. Phys. **A29** (2014) 1450162.
- [18] M. Bordone, D. Buttazzo, G. Isidori and J. Monnard, Eur. Phys. J. **C77** (2017) 618.

- [19] C. Bobeth and A.J. Buras, JHEP **02** (2018) 101.
- [20] S. Fajfer, N. Kosnik and L. Vale Silva, Eur. Phys. J. **C78** (2018) 275.
- [21] Addendum I to P326, SPSC-2019-039.
- [22] F. Brizioli *et al.* (NA62 collab.), PoS (EPS-HEP2021) 553.
- [23] S. A. Akimenko *et al.* (ISTRA+ collab.), Phys. Atom. Nucl. **70** (2007) 702.
- [24] A. Y. Polyarush *et al.* (OKA collab.), Eur. Phys. J. **C81** (2021) 161.
- [25] B. Kubis, E. H. Muller, J. Gasser, M. Schmid, Eur. Phys. J. **C50** (2007) 557.
- [26] E. Cortina Gil *et al.* (NA62 collab.), Phys. Lett. **B797** (2019) 134794.
- [27] E. Cortina Gil *et al.* (NA62 collab.), Phys. Rev. Lett. **127** (2021) 131802.
- [28] E. Cortina Gil *et al.* (NA62 collab.), CERN-EP-2022-018, arXiv:2202.00331, submitted to Phys. Lett. B.
- [29] E. Cortina Gil *et al.* (NA62 collab.), Phys. Lett. **B807** (2020) 135599.
- [30] E. Cortina Gil *et al.* (NA62 collab.), Phys. Lett. **B816** (2021) 136259.
- [31] E. Cortina Gil *et al.* (NA62 collab.), JHEP **02** (2021) 201.
- [32] E. Goudzovski *et al.*, arXiv:2201.07805, submitted to Rep. Prog. Phys.
- [33] M. Rosenthal, *et al.* Int. J. Mod. Phys. **A34** (2019) no.36, 1942026.
- [34] K. Massri, 2021 [Contribution to Physics Beyond Colliders General WG meeting](#).
- [35] B. Döbrich, F. Ertas, F. Kahlhoefer and T. Spadaro, Phys. Lett. **B790** (2019) 537.